A rigidity penalty term for nonrigid registration

Marius Staring,[a] Stefan Klein, and Josien P. W. Pluim
University Medical Center Utrecht, Image Sciences Institute, Q0S.459, P.O. Box 85500, 3508 GA Utrecht, The Netherlands

(Received 14 December 2006; revised 15 June 2007; accepted for publication 18 July 2007; published 10 October 2007)

Medical images that are to be registered for clinical application often contain both structures that deform and ones that remain rigid. Nonrigid registration algorithms that do not model properties of different tissue types may result in deformations of rigid structures. In this article a local rigidity penalty term is proposed which is included in the registration function in order to penalize the deformation of rigid objects. This term can be used for any representation of the deformation field capable of modelling locally rigid transformations. By using a B-spline representation of the deformation field, a fast algorithm can be devised. The proposed method is compared with an unconstrained nonrigid registration algorithm. It is evaluated on clinical three-dimensional CT follow-up data of the thorax and on two-dimensional DSA image sequences. The results show that nonrigid registration using the proposed rigidity penalty term is capable of nonrigidly aligning images, while keeping user-defined structures locally rigid. © *2007 American Association of Physicists in Medicine*. [DOI: 10.1118/1.2776236]

Key words: nonrigid registration, mutual information, B-splines, regularization, rigidity penalty term

I. INTRODUCTION

Image registration is an important technique in the field of medical imaging. In many clinical situations several images of a patient are made in order to analyze the patient's situation. These images are acquired with, for example, x-ray scanners, magnetic resonance imaging (MRI) scanners, computed tomography (CT) scanners, and ultrasound scanners, which provide knowledge about the anatomy of the subject. A combination of patient data, monomodal or multimodal, often yields additional clinical information not apparent in the separate images. For this purpose, the spatial relation between the images has to be found. Image registration is the task of finding a spatial one-to-one mapping from voxels in one image to voxels in the other image. Good reviews on the subject are given in Refs. 1–3.

Popular nonrigid image registration algorithms, as described by Rueckert *et al.*[4] and Mattes *et al.*,[5] do not take the rigidity of different tissue types into account. This can lead to undesired effects in three situations:

- *The image contains various tissue types, each with its own mechanical stiffness*. An example is the presence of rigid objects like bones or surgical instruments in a soft tissue region. Not taking into account the spatially varying stiffness during the registration likely results in unwanted distortions of these rigid objects.[6]
- *Structural changes over time* (*e.g., tumor growth*) *need to be visualized*. Differences that are not of interest (e.g., due to breathing or heart beat) should be compensated for by the nonrigid registration, while the relevant differences induced by changes in the objects of interest should be retained. This would lead to a subtraction image from which the relevant changes are immediately clear.
- *The visibility of structures varies between acquisitions*. For instance, in pairs of precontrast and postcontrast images, like angiography images, vessels are visible in one image and not or only partially in the other. Intensity-based registration algorithms are designed to minimize the difference between two images, resulting in compression of the contrast-enhanced structures. Rohlfing *et al.*[7] and Tanner *et al.*[8] report shrinkage of contrast-enhanced breast lesions in MRI. Rohlfing *et al.*[9] report shrinkage for contrast-enhanced vessels in CT-DSA.

In all three situations the objects of interest should be considered as locally rigid by the registration algorithm.

Other possibilities to detect structural changes over time exist. For example, the deformation field as found by nonrigid registration can be analyzed. This is commonly done by looking at the determinant of the Jacobian of the transformation, see Refs. 10 and 11 and references therein. A discussion on the advantages and disadvantages of the two approaches can be found in the literature.[12,13]

Several methods to constrain deformations have been described in the literature. One that is well known and widely used is to employ a regularization term to penalize undesired transformations. Typical regularization terms include the bending energy of a thin plate,[4] the linear elasticity constraint,[14,15] and the incompressibility constraint.[7,16] Methods that specifically enforce *rigidity* on structures have also been proposed. Tanner *et al.*[8] propose to couple the control points of a B-spline deformation to impose rigidity on certain structures. Another approach is taken by Little *et al.*,[17] who use modified basis functions to describe the deformation. At

rigid locations the deformation is constrained. Arsigny *et al.*[18] use multiple rigid transformations on different parts of the image, which they fuse in such a way that the transformation is invertible. Recently, some approaches were published[19,20] in which rigidity is enforced by penalizing deviation of the Jacobian of the transformation from orthonormality.

In this article we propose a novel penalty term that is capable of locally penalizing nonrigid transformations, which we call a rigidity penalty term. It is based on three criteria that a transformation must meet in order to be rigid: The transformation should be affine, and the rotation matrix of the transformation should be orthonormal and proper. Our rigidity penalty term is a weighted combination of three terms, each imposing one of these conditions. While parts of the proposed rigidity penalty proved to be similar or identical to penalty terms used by other authors,[4,7,19,20] we demonstrate that imposing the complete rigidity penalty term performs better than each of the terms separately. First results of the method were published previously.[21] In Sec. II we construct the rigidity penalty term and prove its validity. Nonrigid registration using the rigidity penalty term is compared against a standard unconstrained nonrigid registration algorithm in Sec. III. Special attention is paid to the sensitivity of the results to the choice of the parameters controlling the rigidity penalty term. We end with a discussion and conclusion in Sec. IV.

II. METHOD

Registration of a moving image $I_M(\boldsymbol{x}):\Omega_M\subset\mathbb{R}^d\mapsto\mathbb{R}$ to a fixed image $I_F(\boldsymbol{x}):\Omega_F\subset\mathbb{R}^d\mapsto\mathbb{R}$, both of dimension d, is the problem of finding a displacement $\boldsymbol{u}(\boldsymbol{x})$ that makes $I_M(\boldsymbol{x}+\boldsymbol{u}(\boldsymbol{x}))$ spatially aligned to $I_F(\boldsymbol{x})$. The quality of alignment is defined by a distance or similarity measure $\mathcal{S}$, such as the sum of squared differences (SSD), the correlation ratio, or the mutual information (MI) measure.

Because this problem is ill-posed, a regularization or penalty term $\mathcal{P}$ is often introduced that constrains $\boldsymbol{u}$. The registration problem is formulated as an optimization problem in which the cost function $\mathcal{C}$ is minimized with respect to $\boldsymbol{u}$, with

$$\mathcal{C}[\boldsymbol{u};I_F,I_M]=-\mathcal{S}[\boldsymbol{u};I_F,I_M]+\alpha\mathcal{P}[\boldsymbol{u}], \tag{1}$$

where α weighs similarity against regularity. This formalism is used in many other papers.[4,7,14–16,19] Note that at the minimum of $\mathcal{C}$ the derivatives of the similarity measure and the regularization term are not necessarily zero. Rather, a balance is found between the two, which is influenced by the parameter α. Therefore, the penalty term cannot be regarded as a hard constraint; it is sometimes referred to as a soft constraint.

The regularization term $\mathcal{P}$ cannot only be considered as a way to achieve well-posedness, but also as a way to enforce desirable properties on the transformation. We propose a regularization term $\mathcal{P}^{\text{rigid}}[\boldsymbol{u};I_M]$ that penalizes deformations of rigid objects, which we call the rigidity penalty term. This penalty term can be weighted locally, so that some parts of the image are restricted to rigid movement, while other parts may be penalized partially or may deform freely.

In the following sections we describe the general registration algorithm (Sec. II A), derive the rigidity penalty term (Sec. II B), and describe how this penalty term can be efficiently computed if the deformation field is parameterized by B-splines (Sec. II C).

II.A. Registration algorithm

We employ a registration framework largely based on the papers of Rueckert *et al.*[4] and Mattes *et al.*[5] The deformation field $\boldsymbol{u}$ is parameterized by cubic B-splines,[4] with parameters $\boldsymbol{\mu}$. The similarity measure $\mathcal{S}$ is the mutual information measure implemented according to Thévenaz and Unser:[22]

$$MI(\boldsymbol{\mu};I_F,I_M)=\sum_{\iota\in L_M}\sum_{\kappa\in L_F}p(\iota,\kappa;\boldsymbol{\mu})\log_2\left(\frac{p(\iota,\kappa;\boldsymbol{\mu})}{p_M(\iota;\boldsymbol{\mu})p_F(\kappa)}\right), \tag{2}$$

where L_F and L_M are the sets of histogram bin centers of the fixed and moving image, respectively, p is the joint discrete probability, and p_F and p_M are the marginal discrete probabilities. B-spline Parzen windows are used to estimate the joint probabilities,

$$p(\iota,\kappa;\boldsymbol{\mu})=\frac{1}{|I_F|}\sum_{\boldsymbol{x}_i\in I_F}w_F(\kappa/\sigma_F-I_F(\boldsymbol{x}_i)/\sigma_F)\cdot w_M(\iota/\sigma_M-I_M(\boldsymbol{x}_i+\boldsymbol{u}_{\boldsymbol{\mu}}(\boldsymbol{x}_i))/\sigma_M), \tag{3}$$

with w_F and w_M the fixed and moving Parzen windows, σ_F and σ_M the histogram bin widths, and $\boldsymbol{u}_{\boldsymbol{\mu}}$ the B-spline deformation field. The marginal probabilities are obtained by summing Eq. (3) over κ or ι.

For the optimization of the cost function $\mathcal{C}$, an iterative stochastic gradient descent optimizer is used:

$$\boldsymbol{\mu}_{k+1}=\boldsymbol{\mu}_k-a_k\frac{\partial\mathcal{C}}{\partial\boldsymbol{\mu}}, \tag{4}$$

where $\frac{\partial\mathcal{C}}{\partial\boldsymbol{\mu}}=-\frac{\partial\mathcal{S}}{\partial\boldsymbol{\mu}}+\alpha\frac{\partial\mathcal{P}}{\partial\boldsymbol{\mu}}$, and $a_k>0$ is the size of the step taken in the negative direction of the derivative. Thévenaz and Unser[22] derived an analytical expression for the derivative $\partial\mathcal{S}/\partial\boldsymbol{\mu}$. In this article the analytical expression is evaluated approximately. Instead of evaluating the derivative over all voxels of the fixed image, i.e., taking all $\boldsymbol{x}_i\in I_F$ in Eq. (3), only a randomly chosen subset of I_F is used. This random subset is renewed every iteration. Klein *et al.*[23] showed that using this stochastic gradient descent optimizer the computation time per iteration can be significantly decreased, without affecting the rate of convergence and final precision. In this article, a decaying function of the iteration number k is used for computing the gain factor: $a_k=a/(k+A)^\gamma$, where $a>0$, $A\geq 1$, and $0\leq\gamma\leq 1$ are user-defined constants. This function, and practical guidance for choosing the parameters, is suggested by Spall.[24] A multiresolution approach is taken to avoid local minima, using a Gaussian pyramid with a subsampling factor of 2 in each dimension.

II.B. Construction of the rigidity penalty term

In this section we derive three conditions that must hold for a transformation $\boldsymbol{u}(\boldsymbol{x})+\boldsymbol{x}$ to be a rigid transformation. These three conditions are combined in one penalty term, our rigidity penalty term $\mathcal{P}^{\text{rigid}}[\boldsymbol{u};I_M]$, constructed such that deviation from these three conditions is penalized. For the sake of clarity the penalty term is derived in 2D. The results can be readily extended to 3D, or even nD.

For a displacement field $\boldsymbol{u}$ to be rigid, it must hold that

$$\boldsymbol{u}(\boldsymbol{x})+\boldsymbol{x}=R\boldsymbol{x}+\boldsymbol{t}, \tag{5}$$

with R and $\boldsymbol{t}$ a rotation matrix and a translation vector, respectively. Three conditions on $\boldsymbol{u}(\boldsymbol{x})+\boldsymbol{x}$ can be derived:

affine: A rigid transformation is an affine function in $\boldsymbol{x}$, giving the affinity conditions $\text{AC}_{kij}(\boldsymbol{x})$, which state that the second order derivatives of $\boldsymbol{u}$ to $\boldsymbol{x}$ have to be zero:

$$\text{AC}_{kij}(\boldsymbol{x})=\frac{\partial^2 u_k(\boldsymbol{x})}{\partial x_i\,\partial x_j}=0, \tag{6}$$

for all $k,i,j=1,2$, not counting duplicates. Rueckert *et al.*[4] penalize deviation from this constraint to enforce smoothness.

orthonormality: For the matrix R to be a rotation matrix it must be orthonormal. This defines the orthonormality conditions $\Sigma_{k=1}^{2} r_{ki}r_{kj}=\delta_{ij}$, for all $i,j=1,2$, with r_{ij} the elements of R, and δ_{ij} the Kronecker delta function. From Eq. (5) it follows that $\frac{\partial u_i}{\partial x_j}=r_{ij}-\delta_{ij}$, for all $i,j=1,2$. Hence, the orthonormality conditions OC_{ij} can be rewritten as

$$\text{OC}_{ij}(\boldsymbol{x})=\sum_{k=1}^{2}\left(\frac{\partial u_k(\boldsymbol{x})}{\partial x_i}+\delta_{ki}\right)\left(\frac{\partial u_k(\boldsymbol{x})}{\partial x_j}+\delta_{kj}\right)-\delta_{ij}=0, \tag{7}$$

for all $i,j=1,2$, again not counting duplicates. Note that, since $r_{ij}=\frac{\partial u_i}{\partial x_j}+\delta_{ij}$ [Eq. (5)], the rotation matrix R is the Jacobian of the transformation $\boldsymbol{u}(\boldsymbol{x})+\boldsymbol{x}$. Therefore, the OC term is equal to forcing orthonormality of the Jacobian, which is used in Loeckx *et al.*[19] and Ruan *et al.*[20]

properness: A matrix R satisfying the orthonormality conditions can still be proper or improper, meaning that the determinant can still be either 1 or −1, respectively. An improper orthonormal matrix corresponds to a rotation with an inversion (mirroring). Therefore we need to impose the properness condition $\text{PC}(\boldsymbol{x})=\det(R)-1=0$, with the elements r_{ij} of the matrix R again expressed in derivatives of $\boldsymbol{u}$ to $\boldsymbol{x}$. Note that, since R is the Jacobian of the transformation $\boldsymbol{u}(\boldsymbol{x})+\boldsymbol{x}$, this condition basically amounts to an incompressibility constraint, see also Ref. 7.

We define the rigidity penalty term $\mathcal{P}^{\text{rigid}}[\boldsymbol{u};I_M]$ to be the sum of all these conditions squared. In order to distinguish between rigid and nonrigid tissue, the total penalty term is weighted by a so-called rigidity coefficient $c(\boldsymbol{x})\in[0,1]$ of the tissue type at position $\boldsymbol{x}$. This results in the following expression:

$$\begin{aligned}\mathcal{P}^{\text{rigid}}[\boldsymbol{u};I_M]\triangleq{}&\frac{1}{\Sigma_{\boldsymbol{x}}c(\boldsymbol{x}+\boldsymbol{u}(\boldsymbol{x}))}\sum_{\boldsymbol{x}}c(\boldsymbol{x}+\boldsymbol{u}(\boldsymbol{x}))\\&\times\left\{c_{\text{AC}}\sum_{k,i,j}\text{AC}_{kij}(\boldsymbol{x})^2+c_{\text{OC}}\sum_{i,j}\text{OC}_{ij}(\boldsymbol{x})^2\right.\\&\left.+c_{\text{PC}}\text{PC}(\boldsymbol{x})^2\right\}.\end{aligned} \tag{8}$$

The weights c_{AC}, c_{OC}, and c_{PC} determine the relative strength of each of the three terms. The rigidity coefficient $c(\boldsymbol{x})$ is set to 0 for pixels $\boldsymbol{x}$ in completely nonrigid tissue, and to 1 for rigid tissue. For other tissue types a value of $c(\boldsymbol{x})$ is chosen between 0 and 1. The rigidity coefficient image can be constructed by performing a manual or (semi-) automatic segmentation of structures of interest, after which a rigidity coefficient can be assigned to each segment. For the case of CT images the Hounsfield units themselves may be used, rescaled to the range [0,1], since more rigid tissue usually has a higher attenuation value. This article concerns the registration method, and therefore we use a simple manual segmentation. The rigidity coefficient image only has to be defined on the moving image. The moving image deforms to the fixed image, so specific parts of the moving image should transform in a rigid fashion. Therefore, the regions that correspond to rigid structures have to be defined on the moving image. When computing the derivative $\partial\mathcal{P}/\partial\mu$ we neglect the derivative of $c(\boldsymbol{x}+\boldsymbol{u}(\boldsymbol{x}))$ to $\boldsymbol{u}$, the same way as overlap changes of images are sometimes neglected in registration.[22] Hence, discontinuity of $c(\boldsymbol{x})$ is not an issue here.

The following theorem states the validity of the proposed rigidity constraint. For clarity, we assume that $c(\boldsymbol{x})>0$, on a connected subregion Ω_S of the moving image.

Theorem 1. *$\mathcal{P}^{\text{rigid}}[\boldsymbol{u};I_M]=0$ if and only if the transformation $\boldsymbol{u}(\boldsymbol{x})+\boldsymbol{x}$ is rigid, provided that $c(\boldsymbol{x})>0$, $\forall\boldsymbol{x}\in\Omega_S\subset\Omega_M$.*

Proof. The *if* part is trivial, so we prove the *only if* part. Let $\mathcal{P}^{\text{rigid}}[\boldsymbol{u};I_M]=0$, which is at every location $\boldsymbol{x}$ a sum of three nonnegative terms. Therefore, each of the three terms is zero. Since the first term is zero, all second order derivatives are zero, making $\boldsymbol{u}(\boldsymbol{x})$ affine. Therefore the displacement can be written as $\boldsymbol{u}(\boldsymbol{x})=\tilde{R}\boldsymbol{x}+\boldsymbol{t}$. Given that the second term is zero it holds that

$$\sum_{k=1}^{2}(\tilde{r}_{ki}+\delta_{ki})(\tilde{r}_{kj}+\delta_{kj})=\delta_{ij},\qquad\forall\,i,j=1,2, \tag{9}$$

since $\frac{\partial u_i}{\partial x_j}=\tilde{r}_{ij}$. Now splitting up $\tilde{R}=R-I_d$ (giving a displacement $\boldsymbol{u}(\boldsymbol{x})=R\boldsymbol{x}-\boldsymbol{x}+\boldsymbol{t}$), gives $\tilde{r}_{ij}=r_{ij}-\delta_{ij}$. Substituting this in Eq. (9) results in $\Sigma_{k=1}^{2}r_{ki}r_{kj}=\delta_{ij}$, $\forall i,j=1,2$, in which we recognize the orthonormality conditions for R. A similar argument holds for the third term, resulting in the properness condition. Therefore R is a rotation matrix, and $\boldsymbol{u}(\boldsymbol{x})+\boldsymbol{x}$ represents a rigid transformation. □

For every application the parameters c_{AC}, c_{OC}, and c_{PC} have to be tuned. A suitable first estimate for those values is

the energy of the three terms after unconstrained registration, relative to each other. The energy of AC is defined as

$$E_{\mathrm{AC}} = \frac{1}{\sum c(\boldsymbol{x}+\boldsymbol{u}(\boldsymbol{x}))} \sum_{\boldsymbol{x}} c(\boldsymbol{x}+\boldsymbol{u}(\boldsymbol{x})) \sum_{k,i,j} \mathrm{AC}_{kij}(\boldsymbol{x})^2. \tag{10}$$

E_{OC} and E_{PC} are defined similarly. We have found that a ratio in the order $c_{\mathrm{AC}}:c_{\mathrm{OC}}:c_{\mathrm{PC}}=100:1:10$ is a good starting point. The results did not appear to be overly sensitive to the choice of the parameters, as discussed in Sec. III.

Provided that no mirroring occurs the OC term is a sufficient condition for local rigidity.[19,20] In the experiments OC per se is explicitly compared with the complete penalty term.

II.C. Using B-splines

The proposed rigidity penalty term is not dependent on a parameterization of the displacement field. We employ a B-spline parameterization, because of the computational benefits. Parameterizing the displacement field $\boldsymbol{u}(\boldsymbol{x})$ by cubic B-splines yields in two dimensions

$$u_i(x_1,x_2) = \sum_{l \in V_{\boldsymbol{x}}} \mu_{li} \beta^3(x_1 - x_{l1}) \beta^3(x_2 - x_{l2}), \tag{11}$$

for all $i=1,2$, with $\beta^3(x)$ the cubic B-spline polynomial, μ_{li} the B-spline coefficients, and $V_{\boldsymbol{x}}$ the set of all control points within the compact support of the B-spline at $\boldsymbol{x}$. It is well known[25] that the derivatives of $\boldsymbol{u}(\boldsymbol{x})$ can also be expressed in terms of the B-spline coefficients, using the rule $\frac{\mathrm{d}\beta^n(x)}{\mathrm{d}x} = \beta^{n-1}(x+\frac{1}{2}) - \beta^{n-1}(x-\frac{1}{2})$. Therefore, $\mathcal{P}^{\mathrm{rigid}}[\boldsymbol{u};I_M]$ can be expressed in terms of the B-spline coefficients μ_{li}. We evaluate the rigidity constraint over the control points only, which imposes local rigidity of the control point grid. Rigidity of the control points in the B-spline support region of an object guarantees rigidity of the entire object. Evaluating over the control points only, combined with the compact support of B-splines, gives us an efficient way to calculate $\mathcal{P}^{\mathrm{rigid}}[\boldsymbol{u};I_M]$ and its derivatives, needed for gradient descent like optimizers.

In order to define a rigid transformation at some point $\boldsymbol{x}$, all control points within the compact support of the B-spline have to be kept rigid. The nonrigid deformation in the neighborhood of a rigid structure is therefore also penalized to some extent. The precision with which a rigid region can be defined, is determined by the density of the B-spline control point grid and the order of the B-spline.

II.D. Synthetic example

To illustrate the effect of the three terms in Eq. (8) we have constructed a synthetic example of size 512×512 pixels, see Fig. 1. The ellipsoid in the fixed image in Fig. 1(a) is rotated and anisotropically scaled compared to the moving image. It represents a tumor that has grown. The rectangle is only rotated and represents a rigid object, such as a bone. The bar is an example of a structure visible in only one of the images, representing a situation before and after contrast uptake in a vessel. The desired behavior of a registration algorithm is that all three objects are kept rigid. Therefore, $c(\boldsymbol{x})=1.0$ on the three objects and zero elsewhere. The resulting rigidity coefficient image is dilated with a kernel of radius 8.0 pixels (two control point spacings). The other parameters in Eq. (8) for this experiment are $\alpha=1.0$, $c_{\mathrm{AC}}=250.0$, $c_{\mathrm{OC}}=2.0$, and $c_{\mathrm{PC}}=10.0$. A B-spline control point spacing of 4.0 pixels is used.

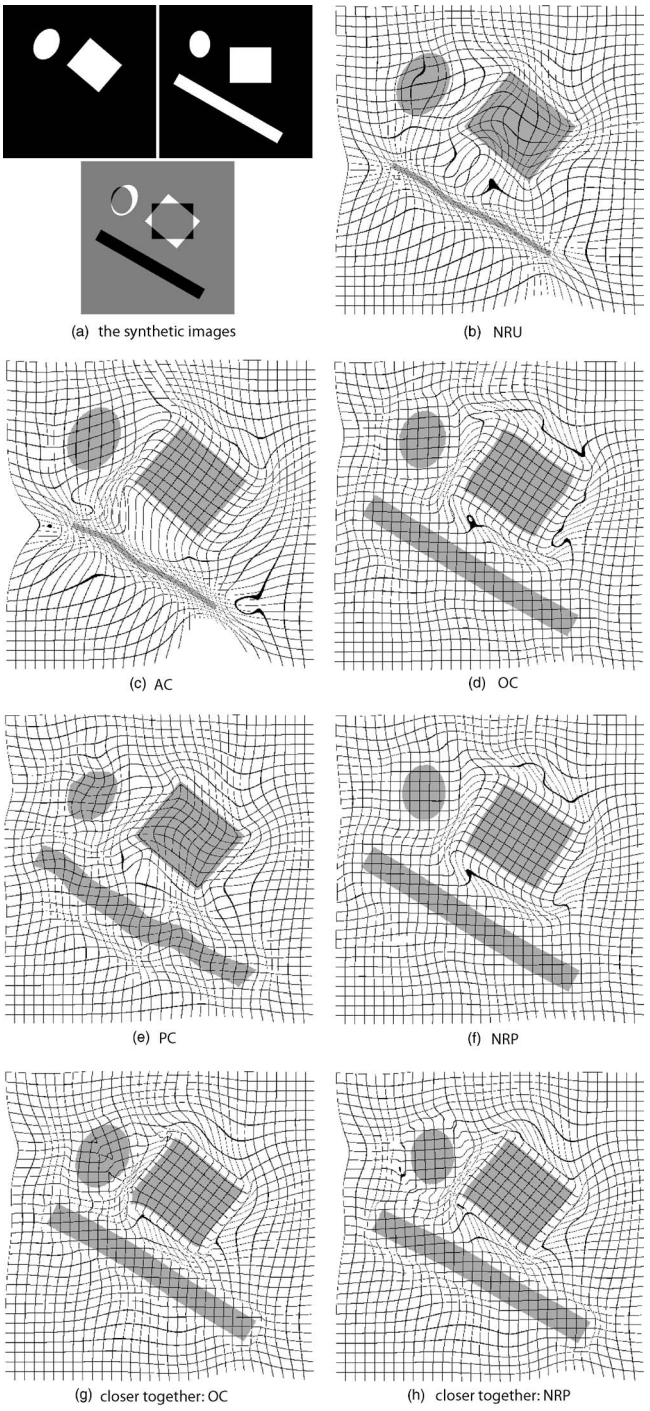

FIG. 1. Illustrating the different parts of the penalty term. (a) Fixed and moving images are shown, together with their difference. The other images show the result after registration using the various methods. (g) and (h) show the result of OC and NRP, respectively, when the objects are placed a little closer together.

TABLE I. The energy E of the three conditions.

Method	E_{AC}	E_{OC}	E_{PC}
NRU	1.9×10^{-3}	$3.4\times10^{+1}$	3.6×10^{0}
AC	5.6×10^{-6}	$3.0\times10^{+1}$	3.6×10^{0}
OC	3.6×10^{-5}	8.6×10^{-3}	2.9×10^{-3}
PC	4.8×10^{-4}	6.3×10^{-1}	2.9×10^{-4}
NRP	1.4×10^{-6}	1.1×10^{-3}	1.3×10^{-4}

In the remainder of this article the abbreviation "NRP" is used for registration with the rigidity penalty term $\mathcal{P}^{\text{rigid}}[\boldsymbol{u};I_M]$ and "NRU" for unconstrained nonrigid registration (only a similarity term). When only one of the conditions in Eq. (8) is used, the method is referred to as "AC," "OC," or "PC."

The NRU algorithm, see Fig. 1(b), registers the ellipsoid and the rectangle, and tries to eliminate the bar, since it is not visible in the fixed image. Note that the outer border of the rectangle is registered correctly, but the deformation field within the object is not rigid at all. When only AC is applied as in Fig. 1(c), the deformations are affine at the three objects, but not rigid, since scaling is not penalized. The orthonormality condition nicely preserves rigidity, see Fig. 1(d). The PC term is volume preserving (Fig. 1(e)), but volume preservation is not equal to rigidity. Finally, in Fig. 1(f), the combination of all terms is used. Rigidity of the three objects is achieved, and the deformation field looks slightly smoother than that of OC alone. Note, that the major axes of the ellipsoids are not aligned in some cases. This is due to the fact that the similarity measure has a constant value for a range of inclination angles, as long as the smaller ellipsoid fits entirely in the larger one.

When the three objects are placed somewhat closer together OC alone is unable to reach the optimum, resulting in a failed registration (the ellipsoid and the rectangle are not rigid, the rectangles do not match completely), see Fig. 1(g). The use of all terms gives a smoother deformation field, and also a good registration, see Fig. 1(h). Note that when the objects are placed closer together some folding appears. This is a consequence of the use of B-splines: Invertibility of the deformation field is not guaranteed. Since the rigidity penalty term is independent of the representation of the deformation field, it can also be applied in combination with a diffeomorphic transformation model.

In Table I the energies of the three components are given for the several registrations of Fig. 1. Together they form a measure of rigidity, since Theorem 1 states that each of them is zero in case of rigidity. The three conditions help each other in achieving rigidity, OC is the most dominant of the three, and the total rigidity term yields the best results.

III. EXPERIMENTS AND RESULTS

In order to evaluate the effectiveness of the rigidity penalty term Eq. (8), NRP was compared to NRU. Additionally, all registrations were performed with only the AC, OC, or PC term as penalty. An appropriate setting for α in Eq. (1) and for the relative strength of each of the terms of $\mathcal{P}^{\text{rigid}}[\boldsymbol{u};I_M]$, controlled by c_{AC}, c_{OC}, and c_{PC}, was determined experimentally. Sensitivity of the results to the relative strength of each term was also investigated.

The methods were compared on clinical data, viz., 3D CT follow-up data of the thorax containing lung tumors (Sec. III A), and 2D digital subtraction angiography (DSA) image data, see Sec. III B.

Throughout this article a 32×32 joint histogram was used to estimate the mutual information. The parameters A and γ, needed to compute the gain factor a_k in Eq. (4), were set to $A=100.0$ and $\gamma=0.602$, see Ref. 24. All experiments were performed with software developed by the authors (www.isi.uu.nl/Elastix). This registration package is largely based on the Insight Segmentation and Registration Toolkit.[26] The computation time for the rigidity penalty term scales linearly with the number of B-spline parameters, and is about 0.06 s for 10 000 parameters in two dimensions and about 3 s for 100 000 parameters in three dimensions, on a standard computer (AMD Opteron 250 running on 2.4 GHz). The calculation of the derivative of the mutual information in 2D and 3D requires 0.11 and 1 s, respectively.

III.A. 3D CT thorax data with lung tumors

A possible way to follow disease progress over time is to visually inspect the difference between a first scan, taken at t_0, and a registered second follow-up scan, taken at t_1. For the case of patients with lung tumors, this difference will indicate tumor growth between two scans. Because of differences in lung inspiration levels, rigid registration is not sufficient to achieve good alignment of the anatomy. However, standard nonrigid registration methods will minimize the difference between tumors at different time points, effectively concealing tumor growth, see Fig. 2(c). Therefore, the tumors should be considered rigid tissue by the nonrigid registration algorithm. Rigidity is evaluated with tumor volume measurements.

III.A.1. Data description

Registration was performed on CT follow-up data sets of the thorax of five patients having lung tumors. For each patient two or three images of different time points were available, such that in total seven registrations were performed. The data were acquired with a Philips 16-slice spiral CT scanner (Mx8000 IDT 16). The images have slices of 512 by 512 voxels. The number of slices varies for the data sets, ranging from 400 to 550. The in-plane voxel size is around 0.7×0.7 mm. Slice thickness is always 1.0 mm, and slices were reconstructed every 0.7 mm. Before registration, each data set was downsampled with a factor of 2 in each dimension to reduce computer memory and computational load. Downsampling was performed by discarding odd rows, columns, and slices. The five data sets contain 30 tumors in total at time t_0, with an average volume of 2.5 ml for the first scan t_0 and 5.1 ml for the follow-up t_1. No new tumors had developed at t_1.

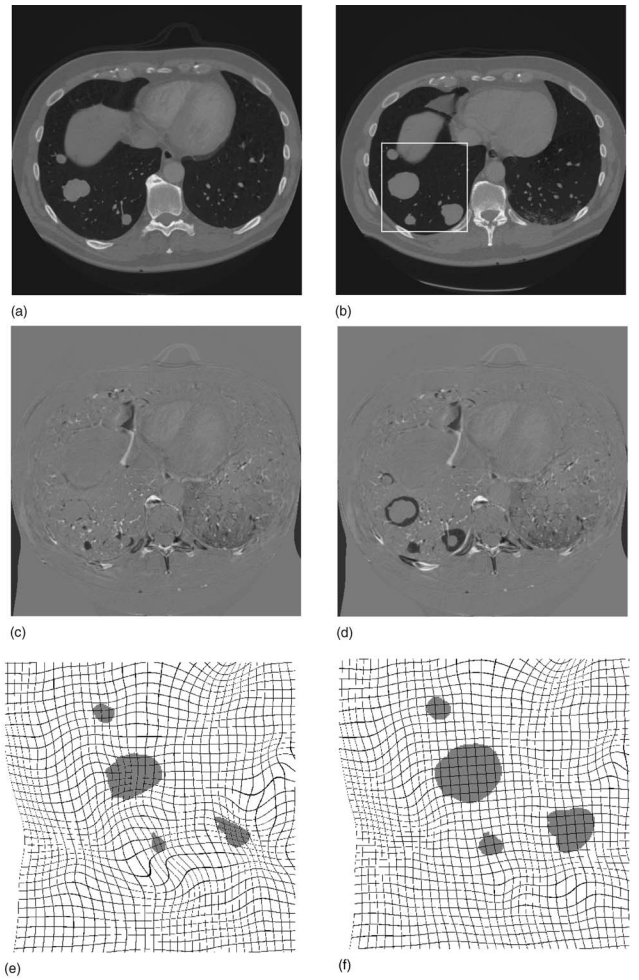

FIG. 2. Comparison of NRU and NRP for a slice taken from 3D CT thorax images. The tumors, located within the box [see (b)], are to be kept rigid. (a) and (b) CT slice at time t_0 (the fixed image) and time t_1 (the moving image), respectively; (c) and (d) difference of the registration result with the fixed image, for NRU and NRP, respectively; (e) and (f) resulting deformation field near the tumors for NRU and NRP, respectively.

III.A.2. Experiment setup

The CT image taken at time t_0 was set to be the fixed image. The CT image taken at time t_1 was used as the moving image. A coarse alignment between fixed and moving image was obtained by a rigid registration. For the rigid registration three resolutions were used, for the nonrigid registration four. For nonrigid registration the resolution of the B-spline grid is adapted each resolution: for the four resolutions the grid spacing was set to 64, 32, 16, and 8 voxels, respectively. The number of optimization iterations for the first three resolutions was 300, for the last one 1200. For every iteration 5000 samples were used to calculate the derivative of the mutual information. The parameter a in the gain factor [see below (4)] was set to 150 000, 120 000, 70 000, and 20 000, for the four resolutions, respectively. For the nonrigid registrations using the rigidity penalty term, a crude manual segmentation of the tumors was used to define $c(\boldsymbol{x})$, setting $c(\boldsymbol{x})$ to 1.0 for voxels within the tumor and to 0.0 elsewhere. The weight α was set to 4.0, and the weights of the three terms were chosen $c_{\mathrm{AC}}=100.0$, $c_{\mathrm{OC}}=1.0$, and $c_{\mathrm{PC}}=2.0$. In the final resolution the rigidity coefficient image was dilated with a radius of 16 voxels (two B-spline control points) to achieve (almost) complete rigidity of the tumors, as discussed in Sec.II C.

III.A.3. Results

As can be seen from Figs. 2(c) and 2(e), NRU fails to keep the tumors rigid. Therefore, the difference in size due to growth cannot be appreciated. Using a crude segmentation of the tumors, NRP succeeds in keeping the tumors rigid, see the deformation field in Fig. 2(f). From the difference image in Fig. 2(d) it is immediately clear that the tumors have grown, whereas the rest of the image was registered with equal accuracy as for the unconstrained nonrigid registration.

The accuracy of the registration was measured by calculating the lung overlap of the registered image with the fixed image. For this purpose, automatic lung segmentations were made with an algorithm based on the method by Hu *et al.*,[27] described in detail in Ref. 28. The overlap measure is defined as

$$\text{overlap} \triangleq \frac{2|L_1 \cap L_2|}{|L_1| + |L_2|}, \tag{12}$$

where L_i is the set of all voxels within the lung, and $|L_i|$ denotes the size of set L_i. The averages and standard deviations of lung overlap were calculated over all data and are

TABLE II. Quantitative results for the 3D CT thorax data. The last five columns show the geometric mean and standard deviation of the tumor volume ratios, grouped according to true tumor growth v_{t_1}/v_{t_0}. The number of lung or tumors segmentations the means and standard deviations are based on, is indicated by n.

Method	Lung overlap	$\frac{v_{t_1}}{v_{t_0}}$:all r_{reg}	$\frac{v_{t_1}}{v_{t_0}}:(0,1]$ r_{reg}	$\frac{v_{t_1}}{v_{t_0}}:(1,\frac{3}{2}]$ r_{reg}	$\frac{v_{t_1}}{v_{t_0}}:(\frac{3}{2},3]$ r_{reg}	$\frac{v_{t_1}}{v_{t_0}}:(3,\infty)$ r_{reg}
rigid	0.93±0.05	0.99×/1.05	0.99×/1.01	0.96×/1.08	0.99×/1.03	1.02×/1.05
NRU	0.97±0.01	0.78×/1.24	0.96×/1.04	0.93×/1.06	0.73×/1.15	0.69×/1.34
AC	0.98±0.01	0.89×/1.16	1.04×/1.05	1.01×/1.11	0.85×/1.12	0.84×/1.16
OC	0.99±0.01	0.96×/1.08	1.02×/1.03	1.00×/1.06	0.96×/1.09	0.91×/1.04
PC	0.98±0.01	0.95×/1.06	0.97×/1.03	1.00×/1.04	0.94×/1.06	0.91×/1.03
NRP	0.99±0.01	0.98×/1.05	1.02×/1.04	1.00×/1.05	0.97×/1.03	0.95×/1.06
n	7	30	3	6	13	8

TABLE III. The arithmetic means and standard deviations of the energy E of the three conditions for the 3D CT thorax data.

Method	E_{AC}	E_{OC}	E_{PC}
NRU	$1.6\times10^{-4}\pm8.3\times10^{-5}$	$1.4\times10^{-1}\pm1.4\times10^{-1}$	$2.8\times10^{-2}\pm3.1\times10^{-2}$
AC	$1.5\times10^{-5}\pm1.7\times10^{-5}$	$9.7\times10^{-2}\pm1.1\times10^{-1}$	$2.3\times10^{-2}\pm3.8\times10^{-2}$
OC	$2.8\times10^{-4}\pm5.1\times10^{-4}$	$7.7\times10^{-3}\pm1.2\times10^{-2}$	$2.2\times10^{-2}\pm5.6\times10^{-2}$
PC	$7.1\times10^{-3}\pm1.1\times10^{-2}$	$6.7\times10^{+0}\pm1.1\times10^{+1}$	$1.5\times10^{-3}\pm1.3\times10^{-3}$
NRP	$5.1\times10^{-6}\pm6.9\times10^{-6}$	$5.2\times10^{-3}\pm7.6\times10^{-3}$	$3.6\times10^{-4}\pm6.2\times10^{-4}$

reported in Table II. The results show that good lung overlap was achieved with all nonrigid registration algorithms. This is confirmed by visual inspection of the results.

For evaluation of the rigidity of the tumors, precise manual segmentations of the tumors were used. Tumor volume measurements were performed to see if the registration is volume preserving, a condition for rigidity. Tumor volume before registration at t_1 is denoted by v_{t_1}; tumor volume after registration with algorithm *reg* is denoted by v_{reg}. The volume after registration was computed by applying the resulting transformation to the manual segmentation of the tumour in the moving image, and subsequently calculating the volume of the transformed segmentation. Volume preservation is expressed by the ratio r_{reg} between the tumor volume after registration and at t_1 (since t_1 is the moving image): $r_{reg}=v_{reg}/v_{t_1}$. If a nonrigid registration is volume preserving for a tumor, then $v_{reg}=v_{t_1}$, and $r_{reg}=1.0$; if a tumor is compressed $r_{reg}<1.0$. For ratios it is better to use the geometric mean μ_g and the geometric standard deviation σ_g, instead of their arithmetic counterparts. This can be easily seen from a small example. Say, we have two ratios 0.5 and 2.0. The arithmetic mean of those two ratios is 1.25, whereas the geometric mean equals 1.0, rating a two time increase in volume equal to a two time decrease. From the definition of the geometric standard deviation it follows that $\sigma_g\geq1$.

The geometric mean volume ratios and standard deviations are reported in Table II, where the symbol $\times/$ is used to indicate the distinction with the arithmetic mean and standard deviation. Geometric means were calculated for four volume ratio groups and for all ratios together. The tumors were grouped according to true tumor growth v_{t_1}/v_{t_0}. The sixth column in Table II, for example, is about the group of tumors with true tumor growth between 3/2 and 3.

It can be appreciated from Table II that volume was much better preserved when applying the rigidity penalty term, compared to unconstrained nonrigid registration. To evaluate the difference in rigidity between NRP and NRU, a statistical test was performed on the logarithm of r_{reg}. The differences of NRP with NRU, are not normally distributed ($p<0.0001$ for Shapiro–Wilk tests). Therefore, we employ the Wilcoxon signed-ranks test. Wilcoxon signed-ranks tests show that NRP is significantly ($p<0.0001$, $n=30$) more rigid than NRU. Volume is by definition preserved for rigid registration. However, the corresponding column in Table II shows that the volume measurements do *not* result in the perfect value $1.0\times/1.0$. This indicates that part of the residual volume difference for all methods can be explained by interpolation artifacts due to resampling when computing v_{reg}. For the nonrigid registration methods, the residual volume difference can also be partially explained by the aforementioned balance (Sec. II) between the intensity-based similarity measure, which yields a force that keeps compressing the tumor, and the rigidity penalty term. This balance can of course be influenced by the parameter α. From Table II it is observed that the separate conditions each are less capable of preserving volume than the combined penalty term. The OC term is again the most dominant term, and performs even better than the PC that penalizes volume changes. The AC term is not volume preserving, since it does not penalize scalings. In Table III, the energies of the different components of the penalty term are reported. It shows that when only one of the conditions is used, the energies of the other terms also decline. The three terms aid each other in achieving rigidity. To evaluate the difference between NRP and OC for rigidity and smoothness (i.e., E_{AC}), a statistical test was performed. For rigidity the test was again performed on the logarithm of r_{reg}. Wilcoxon signed-ranks tests (the data is not normally distributed: $p<0.0001$ for Shapiro–Wilk tests) show that NRP is significantly ($p<0.01$, $n=30$) more rigid than OC; no significant difference was found between the E_{AC}'s of NRP and OC ($p=0.016$, $n=7$). We conclude that nonrigid registration with the total penalty term NRP is best capable of achieving rigidity.

To investigate the sensitivity of the results to the relative importance of each of the three terms of $\mathcal{P}^{\text{rigid}}[\boldsymbol{u};I_M]$, the experiments were repeated while varying the weights c_{AC}, c_{OC}, and c_{PC}. Each of the weights was subsequently increased and decreased by a factor of two, resulting in six additional experiments. The results are given in Table IV, where the three numbers after NRP refer to the setting of the parameters c_{AC}, c_{OC}, and c_{PC}, respectively. For example NRP: $1\frac{1}{2}1$ refers to a registration with the parameter c_{OC} chosen half the original value of 1.0. All other parameter settings were taken equal to NRP above. A Wilcoxon signed-ranks test was used to investigate the difference with NRP in terms of rigidity and smoothness (E_{AC}). No significant difference for rigidity, at a confidence level of $p=0.01$, can be found between NRP and its perturbations, except for NRP: $11\frac{1}{2}$, which is significantly less rigid. No significant difference is found for NRP: $11\frac{3}{4}$. At the same confidence level, no significant difference was found regarding smoothness. We

TABLE IV. Sensitivity of the CT results to the relative importance of the three terms. (+) or (−) means that the method is significantly more respectively less rigid or smooth than NRP using a Wilcoxon signed-ranks test at confidence level $p=0.01$. (=) means that no significant difference is found.

Method	Lung overlap	r_{reg}: all	E_{AC}	E_{OC}	E_{PC}
NRP	0.99±0.01	0.98×/1.05	$5.1\times10^{-6}\pm6.9\times10^{-6}$	$5.2\times10^{-3}\pm7.6\times10^{-3}$	$3.6\times10^{-4}\pm6.2\times10^{-4}$
NRP: $\frac{1}{2}11$	0.97±0.02	0.97×/1.06 (=)	$9.1\times10^{-6}\pm1.2\times10^{-5}$ (=)	$5.4\times10^{-3}\pm7.8\times10^{-3}$	$3.9\times10^{-4}\pm6.5\times10^{-4}$
NRP: $1\frac{1}{2}1$	0.97±0.02	0.98×/1.05 (=)	$5.7\times10^{-6}\pm7.0\times10^{-6}$ (=)	$9.9\times10^{-3}\pm1.3\times10^{-2}$	$4.2\times10^{-4}\pm6.7\times10^{-4}$
NRP: $11\frac{1}{2}$	0.97±0.02	0.96×/1.05 (−)	$4.8\times10^{-6}\pm6.2\times10^{-6}$ (=)	$5.4\times10^{-3}\pm7.8\times10^{-3}$	$6.7\times10^{-4}\pm1.2\times10^{-3}$
NRP: 211	0.97±0.02	0.97×/1.06 (=)	$3.1\times10^{-6}\pm4.2\times10^{-6}$ (=)	$5.1\times10^{-3}\pm7.5\times10^{-3}$	$3.8\times10^{-4}\pm6.5\times10^{-4}$
NRP: 121	0.97±0.02	0.98×/1.05 (=)	$4.1\times10^{-6}\pm5.9\times10^{-6}$ (=)	$2.5\times10^{-3}\pm3.9\times10^{-3}$	$2.7\times10^{-4}\pm4.8\times10^{-4}$
NRP: 112	0.97±0.02	0.97×/1.06 (=)	$5.3\times10^{-6}\pm7.1\times10^{-6}$ (=)	$5.1\times10^{-3}\pm7.4\times10^{-3}$	$1.7\times10^{-4}\pm2.8\times10^{-4}$

conclude that the results are quite robust to the weights of the AC, OC and PC terms relative to each other.

III.B. Digital subtraction angiography

DSA is an established modality for visualizing blood vessels in the human body. During image acquisition patient motion often occurs, due to breathing, heart beat, activity in the intestines, or movement of the body. This motion results in artifacts in the subtraction images. In Fig. 3(c) an example of a subtraction image is shown. Rigid registration is not sufficient in these cases, as shown by the difference image after rigid registration, Fig. 3(d), since 3D rigid motion cannot always be corrected with a 2D rigid transformation of the projection image, and since patient motion is usually of a nonrigid nature.

Typically, in DSA imaging a sequence of images is taken, where different parts of the vasculature are visible at different times. To see the entire imaged vasculature, all the images from this sequence have to be registered to some fixed image. The first image, acquired just before the arrival of the contrast bolus and known as the baseline image, was used as the fixed image. As reported in the literature,[7,8] nonrigid registration of images containing contrast-enhanced structures can lead to significant compression of those structures. See Fig. 3(e) for an example of this behavior. Switching the fixed and the moving image and simply using NRU does not guarantee that compression is avoided. Another disadvantage is that the inverse of the transformation is required. Therefore, a nonrigid registration is required that can treat the vasculature differently from other tissue, to maintain vasculature size.

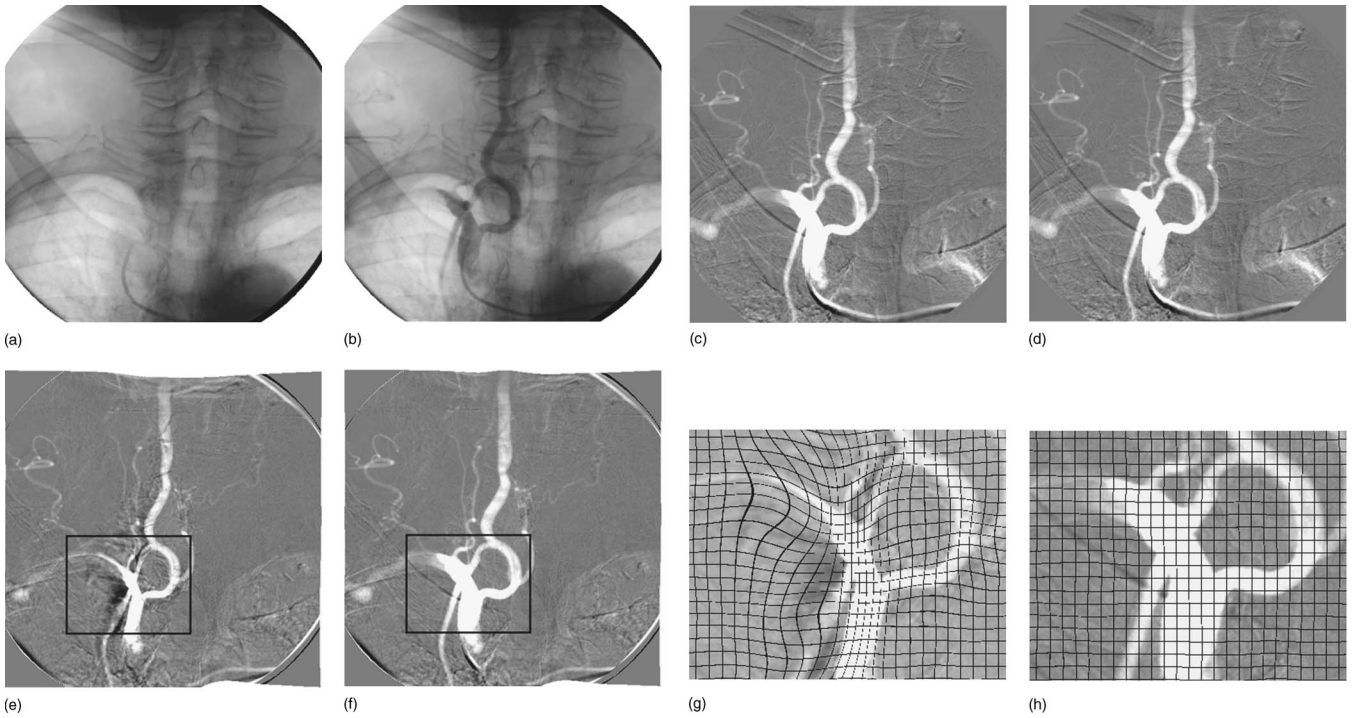

FIG. 3. Comparison of different registration algorithms for 2D DSA images. (a) DSA baseline image, the fixed image; (b) DSA image after injection of the contrast bolus, the moving image; (c)–(f) are difference images of the fixed image, (c) with the moving image, (d) with the result of rigid registration, (e) with the result of NRU, (f) with the result of NRP. (g) and (h) Parts of the resulting deformation field for NRU and NRP, respectively. The rectangles in (e) and (f) denote the part of the deformation field that is depicted.

TABLE V. Quantitative results for the DSA data. Arithmetic means and standard deviations of the RMSD are displayed in the second column. Geometric means and standard deviations of the vessel diameter ratios are shown in the third. The remaining columns show the average values of the three conditions after registration, together with their standard deviation. The last six rows show the sensitivity of the DSA results to the relative importance of the three terms. (+) or (−) means that a method is significantly more or less rigid or smooth, respectively, than NRP using a Wilcoxon signed-ranks test at confidence level $p=0.01$. (=) means that no significant difference is found.

Method	RMSD	r_{reg}	E_{AC}	E_{OC}	E_{PC}
noreg	14.02±5.97				
rigid	13.53±5.73	1.00×/1.00			
NRU	11.94±4.10	0.84×/1.17	$3.7\times10^{-4}\pm2.6\times10^{-4}$	$1.9\times10^{-1}\pm1.2\times10^{-1}$	$4.3\times10^{-2}\pm2.6\times10^{-2}$
AC	12.06±4.38	0.96×/1.05	$3.5\times10^{-6}\pm2.2\times10^{-6}$	$1.8\times10^{-2}\pm1.1\times10^{-2}$	$3.9\times10^{-3}\pm2.3\times10^{-3}$
OC	12.07±4.57	0.98×/1.04	$3.0\times10^{-5}\pm3.0\times10^{-5}$	$6.7\times10^{-4}\pm2.8\times10^{-4}$	$1.1\times10^{-4}\pm5.3\times10^{-5}$
PC	12.13±4.44	0.98×/1.07	$1.3\times10^{-4}\pm1.3\times10^{-4}$	$2.5\times10^{-2}\pm2.2\times10^{-2}$	$1.4\times10^{-5}\pm1.6\times10^{-5}$
NRP	12.18±4.66	0.99×/1.02	$2.5\times10^{-7}\pm1.2\times10^{-7}$	$3.1\times10^{-4}\pm1.5\times10^{-4}$	$7.2\times10^{-6}\pm3.7\times10^{-6}$
NRP: $\frac{1}{2}11$	12.17±4.66	0.99×/1.02 (=)	$5.0\times10^{-7}\pm2.5\times10^{-7}$ (−)	$3.3\times10^{-4}\pm1.6\times10^{-4}$	$7.6\times10^{-6}\pm3.9\times10^{-6}$
NRP: $1\frac{1}{2}1$	12.15±4.64	1.00×/1.02 (=)	$3.7\times10^{-7}\pm1.7\times10^{-7}$ (−)	$6.3\times10^{-4}\pm3.0\times10^{-4}$	$8.9\times10^{-6}\pm5.2\times10^{-6}$
NRP: $11\frac{1}{2}$	12.17±4.66	0.99×/1.02 (=)	$2.6\times10^{-7}\pm1.3\times10^{-7}$ (=)	$3.3\times10^{-4}\pm1.6\times10^{-4}$	$1.7\times10^{-5}\pm8.3\times10^{-6}$
NRP: 211	12.19±4.67	0.99×/1.02 (=)	$1.4\times10^{-7}\pm6.7\times10^{-8}$ (+)	$2.9\times10^{-4}\pm1.5\times10^{-4}$	$7.2\times10^{-6}\pm3.7\times10^{-6}$
NRP: 121	12.21±4.69	1.00×/1.02 (=)	$1.9\times10^{-7}\pm1.0\times10^{-7}$ (+)	$1.4\times10^{-4}\pm7.7\times10^{-5}$	$5.9\times10^{-6}\pm3.0\times10^{-6}$
NRP: 112	12.19±4.67	1.00×/1.02 (=)	$2.7\times10^{-7}\pm1.5\times10^{-7}$ (=)	$3.1\times10^{-4}\pm1.6\times10^{-4}$	$2.8\times10^{-6}\pm1.6\times10^{-6}$

III.B.1. Data description

Two-dimensional digital x-ray angiography image data were acquired with an Integris V3000 C-arm imaging system (Philips). In total, 26 image sequences of 12 different patients were obtained. The image sequences are of size 512×512 pixels for 22 data sets, and 1024×1024 pixels for four data sets; they contain about ten images each. Intensities in the DSA images range approximately from 100 to 950, with an arithmetic mean and standard deviation of about 550±180. Images were taken of different locations in the body: abdomen (10), brain (5), hip and foot (4), heart (1), neck (5), and lungs (1). The first image in each sequence was taken before arrival of the contrast bolus; the following images each show a part of the vasculature.

III.B.2. Experiment setup

The baseline image was taken to be the fixed image. For our experiments one image from each sequence was registered to its fixed image. The image showing the most vasculature was manually selected. To get a coarse alignment between fixed and moving image, a rigid registration was performed prior to nonrigid registration. For nonrigid registration, two resolutions were used, with a B-spline grid spacing of 16 pixels for both resolution levels. For both resolutions, 600 iterations were used. For every resolution 5000 samples were used to calculate the derivative of the mutual information. The parameter a was set to 6000.0 and 3500.0, for the respective resolutions. For the rigidity penalty term, a crude manual segmentation of the vessels was used to define $c(\boldsymbol{x})$, setting $c(\boldsymbol{x})$ to 1.0 for voxels within the vasculature and to 0.0 otherwise. The weight α was set to 8.0, and the weights of the three terms were chosen $c_{AC}=250.0$, $c_{OC}=1.0$, and $c_{PC}=10.0$. The rigidity coefficient image was dilated with a radius of 16.0 pixels to achieve complete rigidity of the vasculature.

III.B.3. Results

The root mean square difference (RMSD) of the background was calculated to verify that the nonrigid registration indeed reduces motion artifacts. The background is defined as everything within the cone beam, but outside the manual vessel segmentation. Arithmetic means and standard deviations of the RMSD were calculated for all 26 images. The results are reported in the second column of Table V and show that rigid registration reduces the motion artifacts only slightly. All nonrigid registration methods improve on that.

In order to further compare the reduction in motion artifacts between the different registration methods, the difference of the RMSDs is calculated as $\mathcal{D}_{i,j}=\mathrm{RMSD}_i-\mathrm{RMSD}_j$, where $i\neq j$ are the different registration methods. This difference was calculated for several combinations of registration methods and for all DSA data. A statistical t test was performed to test the hypothesis that the difference has a zero mean. For the difference $\mathcal{D}_{\mathrm{rigid,noreg}}$ this hypothesis is rejected ($p<0.01$, $n=26$). The difference of any of the nonrigid registration algorithms with rigid registration was also significant ($p<0.005$). No significant difference was found between NRU and the several nonrigid registration algorithms with a penalty term ($p>0.2$). It is clear that rigid registration reduces the motion artifacts slightly, compared to no registration. Nonrigid registration improves substantially on rigid registration.

Visual inspection confirms the reduction in motion artifacts, as measured by the RMSD. An example of this is shown in Fig. 3, where the difference images before registration, after rigid registration, and after NRU and NRP are shown. Compression is clearly visible for NRU [Fig. 3(e)], whereas the vessels for NRP in Fig. 3(f) are similar to the image without registration, Fig. 3(c). The deformation fields in Figs. 3(g) and 3(h) show that NRU compresses the vessels, whereas the rigidity penalty term preserves rigidity.

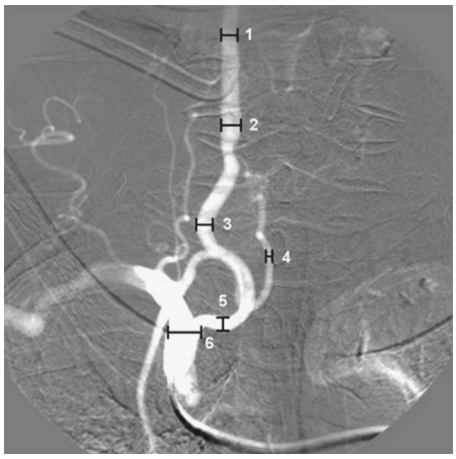

FIG. 4. An example of six locations where the vessel diameter is measured.

The rigidity of the vasculature was evaluated by manually measuring the vessel diameter *vd* at several locations, see Fig. 4 for an example. Six locations were selected for each of the 26 images, yielding a total of 156 diameter measurements. Similar to the tumor volumes in the previous section, ratios r are used to evaluate vessel compression. The vessel diameter after registration is compared to the diameter before registration: $r_{reg}=vd_{reg}/vd_{\mathrm{noreg}}$. The geometric mean and standard deviation of the vessel diameter ratios are reported in the third column of Table V. Unconstrained nonrigid registration (NRU) severely compresses the vasculature, which is avoided with the use of $\mathcal{P}^{\mathrm{rigid}}[\boldsymbol{u};I_M]$ (NRP). A Wilcoxon signed-ranks test confirms that this difference is significant ($p<0.001$, $n=156$). Each of the three conditions preserves the vessel diameter to a large extent. The AC term performs slightly worse than the other two, and the combination again gives a slight improvement, both in mean and standard deviation. Judging from the last three columns in Table V the three conditions help each other in achieving rigidity. Again, a Wilcoxon signed-ranks test was performed (the data is not normally distributed: $p<0.0001$ for Shapiro–Wilk tests) on the difference $\log r_{\mathrm{NRP}}-\log r_{\mathrm{OC}}$, and on the difference in smoothness (E_{AC}). A significant difference is found for both rigidity ($p<0.01$, $n=156$) and smoothness ($p<0.01$, $n=26$), showing that the combination of all terms performs best.

Experiments were repeated with c_{AC}, c_{OC}, c_{PC} halved and doubled. The results are shown in the last six rows of Table V. Changing the relative importance of the three terms does not change the vessel rigidity significantly (using a Wilcoxon signed-ranks test). Smoothness is sometimes significantly different from NRP, see column E_{AC} in Table V, but is still of the order of 10^{-7}.

IV. CONCLUSIONS AND DISCUSSION

We have proposed a novel method to keep user-defined structures locally rigid, while performing nonrigid registration. This is achieved by including a rigidity penalty term, derived from three rigidity conditions, in the registration cost function.

The method was evaluated on 2D and 3D clinical data. It was compared against an unconstrained nonrigid registration approach. From the experiments on CT thorax follow-up data it is observed that tumor volume is preserved when applying the rigidity penalty term, in contrast with unconstrained nonrigid registration. The results on the DSA data show that vessel width is also much better retained with the rigidity penalty term.

The rigidity penalty term consists of three terms: An affinity, an orthonormality, and a properness condition. If used separately, both the properness and the orthonormality condition are to a large extent capable of achieving volume preservation. The affinity condition aids in regularizing the problem. The affinity and properness conditions are by themselves not capable of achieving rigidity. The orthonormality condition is the most dominant of the three terms. The three terms aid each other in achieving rigidity, giving better results than a single condition. Also, the results are quite robust to changing the relative importance of each of the terms. In conclusion, the combination of all terms is the best choice.

Unlike the algorithm described by Tanner *et al.*,[8] the proposed method does not rely on the assumption that the rotation of the rigid object was captured by the initial registration. The rigidity penalty term is suitable for any transformation capable of modelling locally rigid transformations and therefore does not rely on particular basis functions to describe the transformation,[17] or on its specific design.[18] Compared to approaches that take into account only the orthonormality of the Jacobian of the transformation,[19,20] we have shown that the proposed method gives better results in terms of achieving rigidity and smoothness of the resulting deformation field. Since a B-spline parameterization of the deformation field is used, the ability to model local deformations is limited by the B-spline control point spacing. Therefore, segmentation errors in the rigidity coefficient image are a minor problem, as long as they remain smaller than approximately half the control point spacing.

We conclude that nonrigid registration using the proposed rigidity penalty term is capable of nonrigidly aligning images, while keeping user-defined structures locally rigid.

ACKNOWLEDGMENTS

This research was funded by the Netherlands Organisation for Scientific Research (NWO). This work also benefited from the use of the Insight Segmentation and Registration Toolkit (ITK), an open source software package developed as an initiative of the U.S. National Library of Medicine and available at www.itk.org.

[a]Author to whom correspondence should be addressed. Electronic mail: marius@isi.uu.nl

[1]D. L. G. Hill, P. G. Batchelor, M. Holden, and D. J. Hawkes, "Medical image registration," Phys. Med. Biol. **46**, R1–R45 (2001).
[2]H. Lester and S. R. Arridge, "A survey of hierarchical non-linear medical image registration," Pattern Recogn. **32**, 129–149 (1999).
[3]J. B. A. Maintz and M. A. Viergever, "A survey of medical image registration," Med. Image Anal **2**, 1–36 (1998).

[4]D. Rueckert, L. I. Sonoda, C. Hayes, D. L. G. Hill, M. O. Leach, and D. J. Hawkes, "Nonrigid registration using free-form deformations: Application to breast MR images," IEEE Trans. Med. Imaging **18**, 712–721 (1999).
[5]D. Mattes, D. R. Haynor, H. Vesselle, T. K. Lewellen, and W. Eubank, "PET-CT image registration in the chest using free-form deformations," IEEE Trans. Med. Imaging **22**, 120–128 (2003).
[6]M. Staring, S. Klein, and J. P. W. Pluim, "Nonrigid registration with adaptive, content-based filtering of the deformation field," in "SPIE Medical Imaging: Image Processing," in Proc. SPIE Vol. **5747**, 212–221.
[7]T. Rohlfing, C. R. Maurer, Jr., D. A. Bluemke, and M. A. Jacobs, "Volume-preserving non-rigid registration of MR breast images using free-form deformation with an incompressibility constraint," IEEE Trans. Med. Imaging **22**, 730–741 (2003).
[8]C. Tanner, J. A. Schnabel, D. Chung, M. J. Clarkson, D. Rueckert, D. L. G. Hill, and D. J. Hawkes, "Volume and shape preservation of enhancing lesions when applying nonrigid registration to a time series of contrast enhancing MR breast images," in *MICCAI*, Vol. 1935 Lecture Notes in Computer Science, 327–337 (Springer Verlag, Berlin/Heidelberg, 2000).
[9]T. Rohlfing and C. R. Maurer, Jr., "Intensity-based nonrigid registration using adaptive multilevel free-form deformation with an incompressibility constraint," in *MICCAI*, Vol. 2208 Lecture Notes in Computer Science, 111–119 (Springer Verlag, Berlin/Heidelberg, 2001).
[10]D. Rey, G. Subsol, H. Delingette, and N. Ayache, "Automatic detection and segmentation of evolving processes in 3d medical images: Application to multiple sclerosis," Med. Image Anal **6**, 163–179 (2002).
[11]C. Studholme, C. S. Drapaca, B. Iordanova, and V. Cardenas, "Deformation-based mapping of volume change from serial brain MRI in the presence of local tissue contrast change," IEEE Trans. Med. Imaging **25**, 626–639 (2006).
[12]J. Ashburner and K. J. Friston, "Why voxel-based morphometry should be used," Neuroimage **14**, 1238–1243 (2001).
[13]F. L. Bookstein, "Voxel-based morphometry should not be used with imperfectly registered images," Neuroimage **14**, 1454–1462 (2001).
[14]G. E. Christensen and H. J. Johnson, "Consistent image registration," IEEE Trans. Med. Imaging **20**, 568–582 (2001).
[15]B. Fischer and J. Modersitzki, "A unified approach to fast image registration and a new curvature based registration technique," Linear Algebr. Appl. **380**, 107–124 (2004).
[16]E. Haber and J. Modersitzki, "Numerical methods for volume preserving image registration," Inverse Probl. **20**, 1621–1638 (2004).
[17]J. A. Little, D. L. G. Hill, and D. J. Hawkes, "Deformations incorporating rigid structures," Comput. Vis. Image Underst. **66**, 233–232 (1997).
[18]V. Arsigny, X. Pennec, and N. Ayache, "Polyrigid and polyaffine transformations: A novel geometrical tool to deal with non-rigid deformations application to the registration of histological slices," Med. Image Anal **9**, 507–523 (2005).
[19]D. Loeckx, F. Maes, D. Vandermeulen, and P. Suetens, "Nonrigid image registration using free-form deformations with a local rigidity constraint," in *MICCAI*, Vol. 3216 Lecture Notes in Computer Science, 639–646 (Springer Verlag, Berlin/Heidelberg, 2004).
[20]D. Ruan, J. A. Fessler, M. Roberson, J. Balter, and M. Kesler, "Nonrigid registration using reglarization that accomodates local tissue rigidity," in SPIE Medical Imaging: Image Processing, in Proc. SPIE Vol. **6144**, 346–354.
[21]M. Staring, S. Klein, and J. P. W. Pluim, "Nonrigid registration using a rigidity constraint," in SPIE Medical Imaging: Image Processing, in Proc. SPIE Vol. **6144**, 355–364.
[22]C. P. Thévenaz and M. Unser, "Optimization of mutual information for multiresolution image registration," IEEE Trans. Image Process. **9**, 2083–2099 (2000).
[23]S. Klein, M. Staring, and J. P. W. Pluim, "Comparison of gradient approximation techniques for optimisation of mutual information in nonrigid registration," in SPIE Medical Imaging: Image Processing, in Proc. SPIE Vol. **5747** 192–203.
[24]J. C. Spall, "Implementation of the simultaneous perturbation method for stochastic optimization," IEEE Trans. Aerosp. Electron. Syst. **34**, 817–823 (1998).
[25]M. Unser, "Splines: A perfect fit for signal and image processing," IEEE Signal Process. Mag. **16**, 22–38 (1999).
[26]L. Ibáñez, W. Schroeder, L. Ng, and J. Cates, *The ITK Software Guide*, 2nd ed. (Kitware, Inc., New York, 2005), ISBN 1-930934-15-7.
[27]S. Hu, E. A. Hoffman, and J. M. Reinhardt, "Automatic lung segmentation for accurate quantitation of volumetric X-Ray CT images," IEEE Trans. Med. Imaging **20**, 490–498 (2001).
[28]I. C. Sluimer, M. Prokop, and B. van Ginneken, "Towards automated segmentation of the pathological lung in CT," IEEE Trans. Med. Imaging **24**, 1025–1038 (2005).